



Preparation of highly active heterogeneous Au@Pd bimetallic catalyst using plant tannin grafted collagen fiber as the matrix

Jun Ma^{a,b}, Xin Huang^{a,b}, Xuepin Liao^{a,b}, Bi Shi^{a,*}

^a Department of Biomass Chemistry and Engineering, Sichuan University, Chengdu 610065, PR China

^b National Engineering Laboratory for Clean Technology of Leather Manufacture, Sichuan University, Chengdu 610065, PR China

ARTICLE INFO

Article history:

Received 3 March 2012

Received in revised form 18 July 2012

Accepted 22 July 2012

Available online 31 July 2012

Keywords:

Core-shell structure

Metallic catalyst

Bimetallic nanoparticles

Tannin grafted collagen fiber

Liquid-phase hydrogenation

ABSTRACT

Au@Pd bimetallic nanoparticles (NPs) catalysts were synthesized by a seeding growth method using bayberry tannin grafted collagen fiber (BT-CF) as the matrix. In this method, Au³⁺ was first reductively adsorbed onto BT-CF to form Au NPs, and then they serve as the seeds for the over growth of Pd shell. The morphology of BT-CF-Au@Pd catalyst was observed by TEM and SEM, and the core-shell structure of the Au@Pd was confirmed by EDS and XRD. It was found that the as-prepared BT-CF-Au₉@Pd₃ catalyst showed excellent synergy effect in liquid-phase hydrogenation of cyclohexene, whose reaction time was three times faster than that catalyzed by BT-CF-Pd catalyst under the same conditions. Meanwhile, the BT-CF-Au₉@Pd₃ catalyst could be re-used four times without significant loss of activity. In the fourth run, the substrate conversion was still as high as 92.70%, much better than that by using commercial Pd/C catalyst (42.60%). Additionally, BT-CF-Au₉@Pd₃ catalyst exhibited high hydrogenation activity to various alkenes and nitro-compounds. For example, the TOF of allyl alcohol, styrene and nitrobenzene hydrogenations reached 10,980, 14,732 and 1379 mol mol⁻¹ h⁻¹, respectively.

© 2012 Published by Elsevier B.V.

1. Introduction

More recently, core-shell bimetallic NPs have attracted growing interest in the field of catalysis because the catalytic performances of these NPs, including activity and selectivity, can be adjusted by varying the composition, core size and shell thickness [1–3]. In general, the core-shell bimetallic NPs are prepared by a two-step seeding-growth method, where one kind of metallic nanoparticles are first synthesized and then serve as seeds for the overgrowth of secondary metal. According to this method, some kinds of core-shell bimetallic NPs have been successfully synthesized, such as Ru@Pt [4], Rh@Pd [5], Au@Pd [6] and Au@Ag [7].

The core-shell bimetallic NPs are commonly supported by solid matrices through impregnation method so that the heterogeneous catalysts can be obtained. However, although the heterogenization of core-shell bimetallic NPs can be achieved by impregnation method, the supported NPs are somewhat easily detached from the solid matrices owing to the weak interactions between the NPs and the matrices. Moreover, aggregation of NPs may also occur during the reactions. As a result, the catalytic activity of the catalysts is substantially decreased during recycles. Ideally, the bimetallic NPs should be stably anchored onto the solid matrix, which prevents the leakage and aggregation of the metal NPs, thus providing a good

reusability of the catalysts. To fulfill this purpose, it is essentially important to find a suitable matrix that metal NPs can be tightly anchored on.

Plant tannins are soluble polyphenols extracted from plants and have high affinity toward various metal species. In our previous work [8–10], plant tannins were chemically grafted onto collagen fibers, and then, the resultant materials were used as supporting matrices to prepare heterogeneous Pd NPs catalyst. Due to the anchoring effect of plant tannin to the Pd NPs, the leaching of metal species was considerably suppressed during recycles, and accordingly, the catalyst exhibited excellent reusability. Moreover, the as-prepared Pd NPs showed extremely highly catalytic activity due to the fibrous morphology of the supporting matrix. Consequently, it is feasible in principle to prepare highly active and reusable heterogeneous bimetallic NPs catalyst by using plant tannin-grafted collagen fiber as the supporting matrix.

Our recent studies showed that, due to the strong reduction ability of the plant tannins, they were able to directly reduce Au³⁺ to Au NPs in solution, and the formed Au NPs were still well dispersed and stabilized by the plant tannins [11,12]. Furthermore, quantum chemistry calculations suggested that the surface of the Au NPs anchored by plant tannins was negatively charged because of the electron donating-accepting interactions between the plant tannins and the Au NPs [13]. Based on these results, we assumed that these negatively charged Au NPs anchored by the plant tannin grafted-collagen fiber could serve as the *in situ* seeds for the overgrowth of positively charged second metal species, like Pd²⁺.

* Corresponding author. Tel.: +86 28 85400356; fax: +86 28 85400356.

E-mail address: shibitannin@vip.163.com (B. Shi).

Therefore, it can be expected that a highly stable heterogeneous core-shell bimetallic NPs catalyst would be conveniently prepared by a two-step seeding-growth method using plant tannin grafted-collagen fiber as the supporting matrix. In this way, the synthesis of heterogeneous bimetallic Au@Pd NPs would become quite simple since the Au@Pd NPs are *in situ* formed, anchored and dispersed on the plant tannin-grafted collagen fiber, which integrates the procedures of preparation and heterogenization of Au@Pd NPs. However, the implementation of this strategy requires the rational controlling of molar ratio of Au³⁺/Pd²⁺ because Pd²⁺ would be mainly chelated by the phenolic hydroxyls of tannin rather than adsorbed on the surface of Au NPs if the Au³⁺ reductively adsorbed onto the BT-CF does not consume all the phenolic hydroxyls of BT.

To confirm our assumption, bayberry tannin (BT), a kind of condensed tannin, was first grafted onto collagen fiber (CF) using glutaraldehyde as the cross-linking agent. Then, the obtained BT-grafted CF (BT-CF) was used as supporting matrix to reductively adsorb Au³⁺, followed by adsorption and chemical reduction of different amounts of Pd²⁺. All the as-prepared heterogeneous BT-CF anchored Au/Pd NPs (BT-CF-Au/Pd) catalysts were analyzed by TEM and EDS in order to identify the size and structure of the metal NPs. Indeed, heterogeneous BT-CF-Au/Pd catalysts with or without Au@Pd core-shell structure were both prepared by varying the molar ratio of Au³⁺/Pd²⁺. The BT-CF-Au/Pd catalyst with Au core/Pd shell structure (denoted as BT-CF-Au@Pd) was further characterized by XRD and XPS analyses. Subsequently, the catalytic hydrogenations of unsaturated organic compounds were used to evaluate the catalytic activity of the as-prepared catalysts.

2. Experimental

2.1. Reagents

Collagen fiber (CF) was prepared from cattle skin according to our previous work [10]. PdCl₂, HAuCl₄ (99%), borohydride (NaBH₄), glutaraldehyde (50%), and other chemicals were all analytical reagents. Bayberry tannin (BT) was purchased from a plant of forest product in Guangxi Province (China).

2.2. Preparation of BT-grafted CF (BT-CF)

3.0 g of BT was dissolved in 100 mL of distilled water, and then 5.0 g of CF was added. The mixture was stirred at 298 K for 2 h and then filtrated. The collected filter cake was added into 50.0 mL of glutaraldehyde solution (2.0 wt.%) at pH 6.5, and the mixture was stirred at 318 K for 6 h, which allows the chemical grafting of BT onto CF. When the reaction was completed, BT-CF was collected by filtration, fully washed with distilled water and dried in vacuum at 308 K for 12 h. According to the ultraviolet-visible spectra measurement of residual BT in solution, the grafting degree of BT on the BT-CF was determined to be 42.39% in weight.

2.3. Preparation of BT-CF-Au/Pd

1.0 g of BT-CF was suspended in 27.0 mL of HAuCl₄ solution (Au³⁺ = 1.0 g/L, pH = 2.0). The mixture was stirred at 303 K for 4 h, which allows the adsorption and reduction of Au³⁺ onto the BT-CF, resulting in the formation of BT-CF anchored Au NPs (BT-CF-Au). Subsequently, 2.0 mL of PdCl₂ solution (Pd²⁺ = 1.0 g/L) was added into the above mixture, and the pH of the mixture was adjusted to 4.0 using 0.1 M NaOH. The mixture was stirred at 303 K for 4 h in order to adsorb Pd²⁺ onto the BT-CF-Au. After this, the mixture was filtrated and fully washed with deionized water. The filter cake was re-dispersed in 10.0 mL of distilled water, and then 100 mL of 0.1 M NaBH₄ solution was drop-wise added into the solution in order to reduce the Pd²⁺ to Pd(0). Finally, BT-CF-Au₉/Pd₁ catalyst

Table 1

Metal compositions of BT-CF-Au_x/Pd_y, BT-CF-Au and BT-CF-Pd analyzed by ICP-AES.

Samples	Metal composition		
	Au (mmol)	Pd (mmol)	Au/Pd molar ratio
BT-CF-Au ₉ /Pd ₁	2.47	0.28	8.82:1
BT-CF-Au ₉ /Pd ₃	2.50	0.84	8.93:3
BT-CF-Au ₁ /Pd ₁	1.52	1.47	1:1.03
BT-CF-Au	2.50	0	–
BT-CF-Pd	0	2.8	–

was obtained by filtration, followed by fully washed with deionized water and dried in vacuum at 308 K for 24 h. Additionally, the BT-CF-Au₉/Pd₃, and BT-CF-Au₁/Pd₁ catalysts with different molar ratio were prepared, in which the volume of HAuCl₄ solution (1.0 g/L) was 27.0 mL, 10.5 mL, respectively. BT-CF-Au and BT-CF-Pd catalysts were also prepared by the similar procedure as described above. According to the ICP-AES analysis, the actual contents of Pd²⁺ and/or Au³⁺ of all the catalysts were determined, and summarized in Table 1.

2.4. Characterization of catalysts

The surface morphology of the catalysts was observed by Scanning Electron Microscopy (SEM, JEOL LTD JSM-5900LV). X-ray Photoelectron Spectroscopy (XPS, Kratos XSAM-800, UK) analyses were conducted by employing Mg Ka X-radiation ($h\nu = 1253.6$ eV) and a pass energy of 31.5 eV. All of the binding energy peaks of XPS spectra were calibrated by placing the principal C1s binding energy peak at 284.7 eV. The peaks from all high resolution core spectra were fitted by XPSPEAK 4.1 software, using mixed Gaussian-Lorentzian functions. X-ray Diffraction (XRD, Philips X'Pert Pro-MPD) studies were performed to identify the formation of Au/Pd crystal phase by using Cu Ka X-radiation ($\lambda = 0.154$ nm). The size and distribution of Au/Pd NPs on BT-CF were determined using Transmission Electron Microscopy (TEM, FEI-Tecna G2 microscope) operated at an acceleration voltage of 200 kV. The core-shell structure of the BT-CF-Au@Pd catalysts was confirmed using Energy Dispersive Spectroscopy (EDS). Ultra Violet Diffuse Reflectance (UV-DR) Spectroscopy was measured using Varian Cary 5E UV-vis NIR spectrophotometer.

2.5. Catalytic hydrogenation of unsaturated organic compounds

Pd catalysts are commonly used in catalytic hydrogenation of unsaturated organic compounds. Therefore, the catalytic hydrogenation of cyclohexene was employed as a probe reaction to evaluate the catalytic activity and reusability of the BT-CF-Au/Pd catalysts. Briefly, a certain amount of BT-CF-Au/Pd catalyst (containing 2.5 μ mol metal Pd), cyclohexene (10.0 mmol) and methanol (10.0 mL) were introduced into a 50.0 mL stainless steel autoclave equipped with a stirring bar. Then, the catalytic hydrogenation was conducted under 1.0 MPa of H₂ at 298 K, and the obtained products were analyzed by gas chromatography. After reaction, the catalyst was recovered by filtration, thoroughly washed with methanol, and then reused. For comparison, the catalytic hydrogenation of cyclohexene was also carried out under the same experimental conditions using BT-CF-Au, BT-CF-Pd and commercial 5% Pd/C as catalyst, respectively.

In addition, hydrogenations of 2-methyl-3-buten-2-ol, acrylic acid, α -methacrylic acid, styrene, nitrobenzene, *o*-nitrotoluene, and *m*-nitrotoluene catalyzed by BT-CF-Au@Pd catalyst were also carried out to evaluate the universal application of

BT-CF-Au@Pd. The turnover frequency (TOF) of the catalysts was calculated as:

$$\text{TOF}(\text{mol mol}^{-1} \text{h}^{-1}) = \frac{\text{hydrogenated substrate}(\text{mol})}{\text{Pd}(\text{mol}) \times \text{reaction time}(\text{h})}$$

3. Results and discussion

3.1. Preparation of BT-CF-Au/Pd catalysts

The molecular structure of BT is shown in Scheme 1a. It mainly consists of flavan-3-ols, in which the C6 and C8 of the A-rings have high nucleophilic reactivity toward electrophilic reagents, like aldehydes. Additionally, collagen fiber is also able to react with aldehydes via the $-\text{NH}_2$ on its side chains. Therefore, we used glutaraldehyde as the bifunctional cross-linking agent to form bridges between BT and CF, as shown in Scheme 1b. On the other hand, BT has a large number of adjacent phenolic hydroxyls on its B-rings. Our previous study has proved that the phenolic hydroxyls of BT were able to reduce Au^{3+} into Au NPs [13]. Thus, it can be assumed that the BT grafted onto CF can still reduce Au^{3+} to form Au NPs, and the formed Au NPs should also be anchored onto the BT-CF (Scheme 1c). Actually, the UV-DR spectrum of the BT-CF-Au indicated the presence of characteristic absorption peak of Au NPs around 520 nm (supporting information 1), which confirmed the formation of Au NPs on BT-CF.

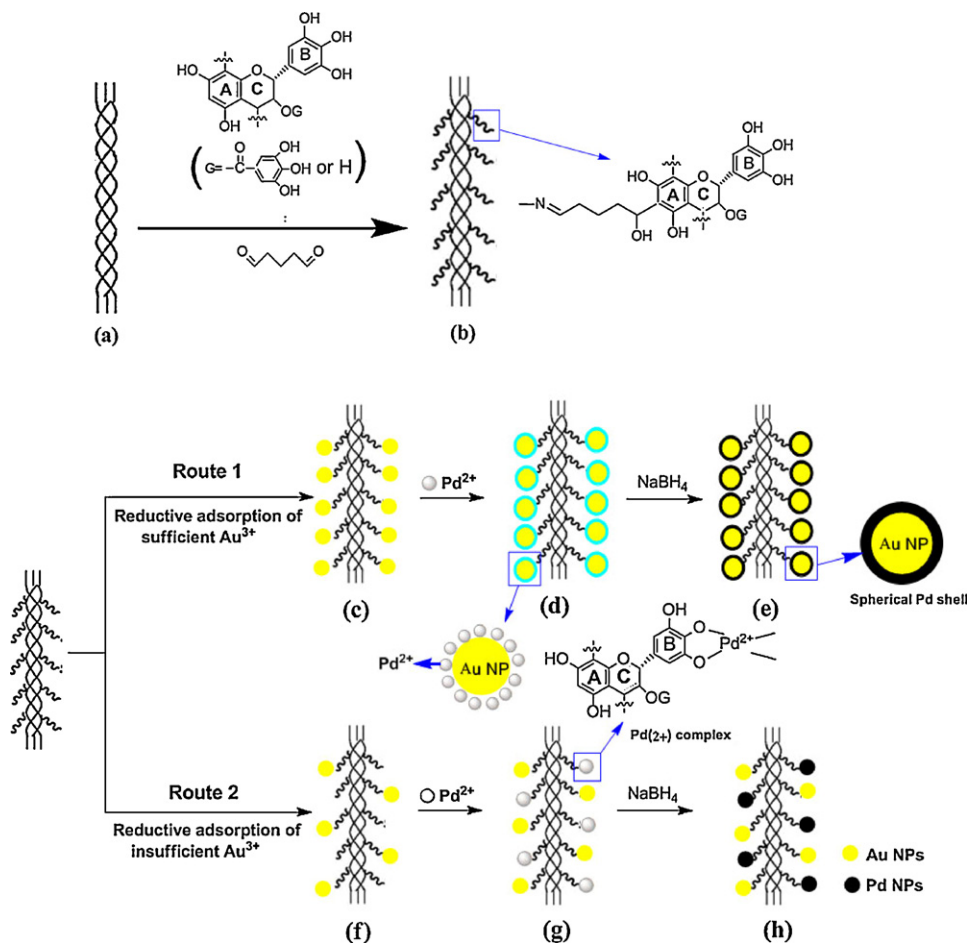
Based on our previous quantum chemistry calculations [13], the Au NPs anchored on BT-CF is negatively charged. Therefore the positively charged Pd^{2+} should be mainly adsorbed on the surface of

Au NPs if the phenolic hydroxyls are consumed by the reductive adsorption of Au^{3+} , as shown in Scheme 1d. After reduction by NaBH_4 , the Pd^{2+} would be reduced to Pd shell over the Au NPs, thus forming the Au@Pd NPs (Scheme 1e). However, Pd^{2+} will be mainly chelated by the phenolic hydroxyls of BT if the amount of Au^{3+} is not sufficient enough to consume the major positions of phenolic hydroxyls of BT (Scheme 1g). Under such conditions, the reduction of Pd^{2+} would lead to the formation of individual Pd NPs and/or the alloy of Au and Pd, instead of Au@Pd core-shell NPs (Scheme 1h).

3.2. Characterization of the catalysts

The morphology and size distribution of the catalysts were determined by Transmission electron micrographs (TEM). TEM images of monometallic BT-CF-Au, BT-CF-Pd NPs and bimetallic BT-CF-Au₁/Pd₁ NPs catalysts are shown in Fig. 1a–c, and the corresponding histograms of particle size distribution are presented in Fig. 1d–f. As shown in Fig. 1a, the NPs in monometallic BT-CF-Au are roughly spherical, and the corresponding particle size are around 10.65 ± 1.2 nm. In Fig. 1b, the monometallic BT-CF-Pd exhibited much smaller Pd particle size with average diameter of 3.72 ± 0.7 nm. However, the spherical NPs in BT-CF-Au₁/Pd₁ appear in uneven distribution, with average sizes located around 9.75 nm and 23.25 nm, respectively. EDS point analyses of distinct NPs in BT-CF-Au₁/Pd₁ were adopted to further identify the composite distribution.

As shown in Fig. 2, the NPs with large diameter in BT-CF-Au₁/Pd₁ are found to be mono-Au NPs. The small NPs are too small to be analyzed by EDS method. However, the above ICP-AES analysis has



Scheme 1. Proposed preparation mechanism of BT-CF-Au/Pd.

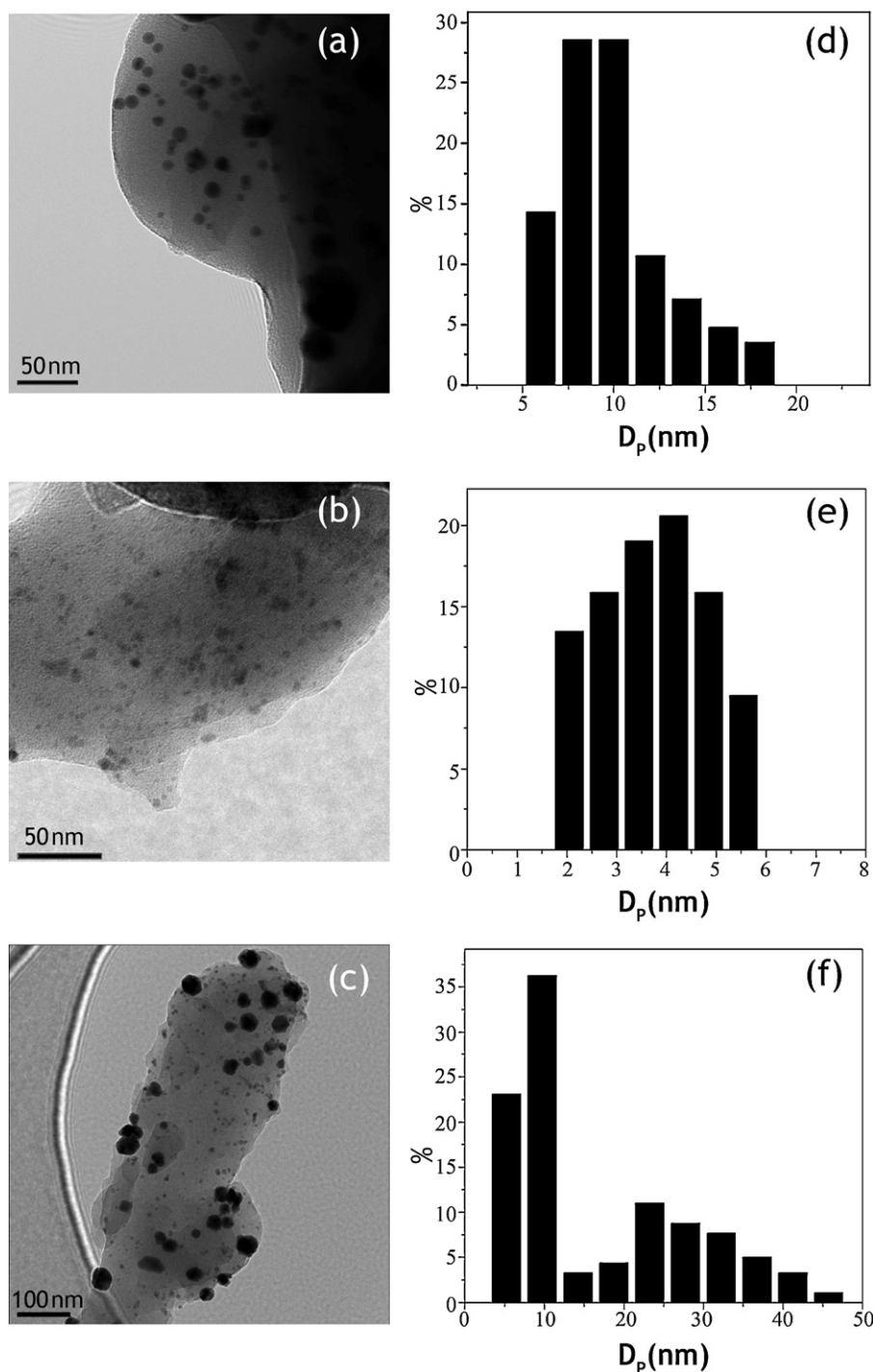


Fig. 1. TEM images of BT-CF-Au (a), BT-CF-Pd (b) and BT-CF-Au₁/Pd₁ (c), and the histograms of size distribution of BT-CF-Au (d), BT-CF-Pd (e) and BT-CF-Au₁/Pd₁ (f).

confirmed that the molar ratio of Pd/Au is close to 1:1. Hence, it is reasoned that the small NPs observed in Fig. 1b should be mono-Pd NPs. That is, when the molar ratio of Au³⁺/Pd²⁺ is 1:1, the reductively adsorbed Au³⁺ on the BT-CF is not enough to consume all the active phenolic hydroxyls, and accordingly, the subsequently adsorbed Pd²⁺ would be mainly chelated by the residual phenolic hydroxyls of BT, and then *in situ* reduced by the addition of NaBH₄ to form individual Pd NPs. Interesting, the Au NPs in BT-CF-Au₁/Pd₁ are relatively larger than those in monometallic BT-CF-Au. Considering the preparation mechanism proposed in Scheme 1, the varied size of Au NPs should be attributed to the differences in reductive growth of Au³⁺ in those catalysts. During the preparation of

BT-CF-Au₁/Pd₁, low amount of Au³⁺ (1.0 g/L, 10.5 mL) was employed to synthesize Au NPs. Under such conditions, a small amount of Au⁰ seeds was initially formed, which further grown to form large Au nanoparticle along with the successive reduction of Au³⁺. However, when high amount of Au³⁺ (1.0 g/L, 27.0 mL) was used for the preparation of BT-CF-Au, the Au⁰ seeds initially formed onto BT-CF were much more than those onto BT-CF-Au₁/Pd₁, and accordingly, the further growth of Au⁰ seeds should be considerably suppressed due to their large numbers. As a result, the use of high amount of Au³⁺ leads to the formation of smaller Au nanoparticles.

TEM image of BT-CF-Au₉/Pd₁ NPs is illustrated in Fig. 3. It is observed that the NPs in BT-CF-Au₉/Pd₁ have an average particle

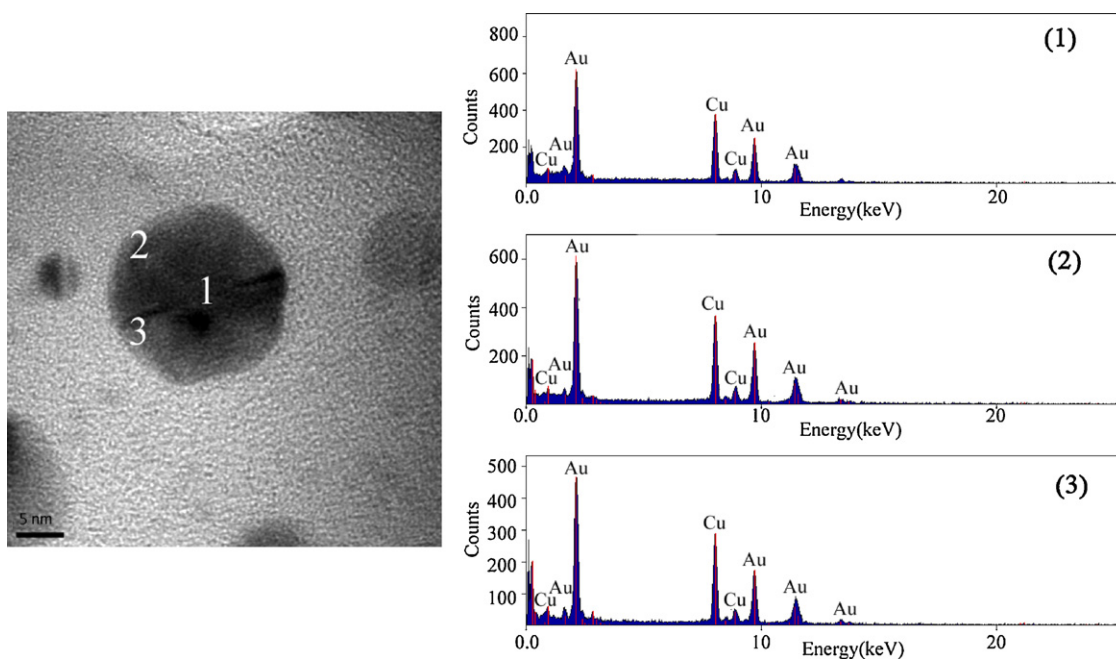


Fig. 2. EDS point analyses of a distinct NP in BT-CF-Au₁/Pd₁.

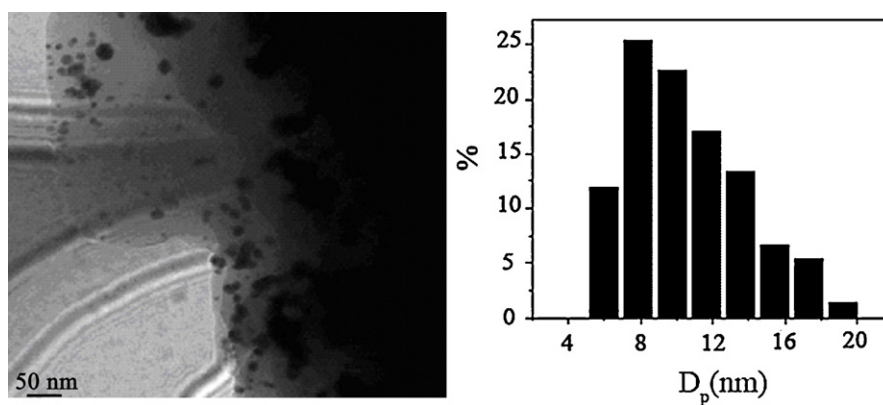


Fig. 3. TEM image and the histogram of size distribution of BT-CF-Au₉/Pd₁.

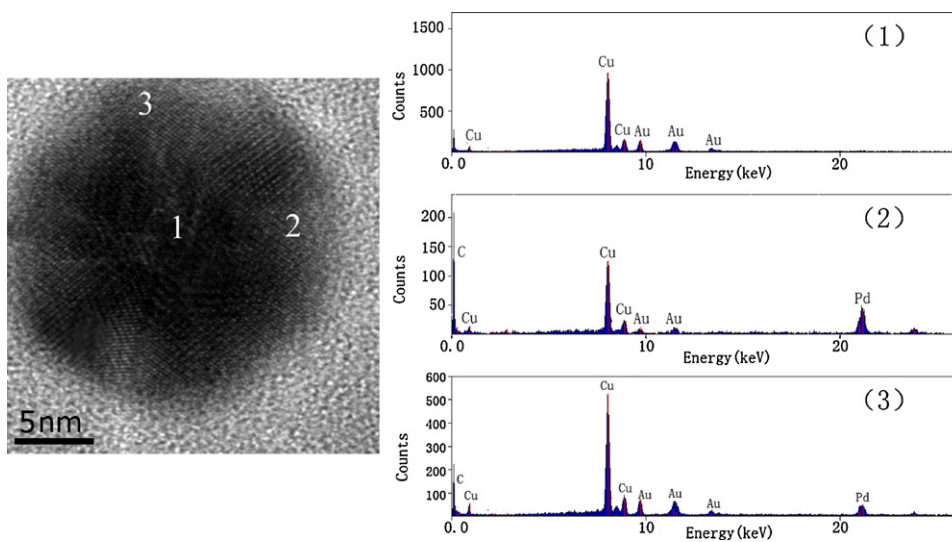


Fig. 4. EDS point analyses of a distinct NP in BT-CF-Au₉/Pd₁.

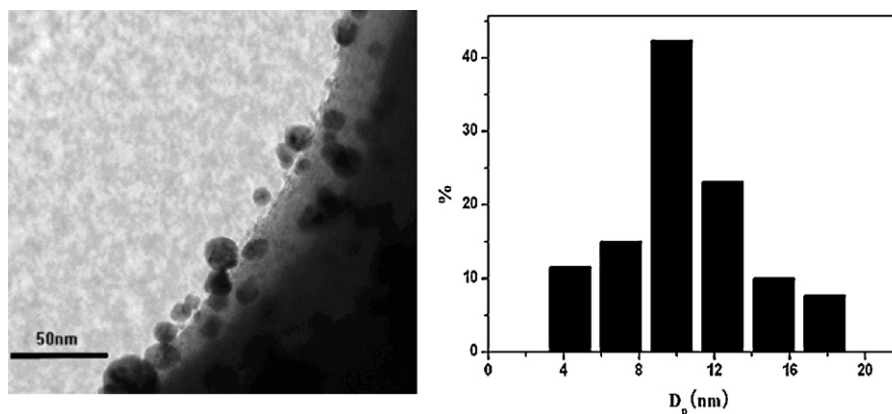


Fig. 5. TEM image and the histogram of size distribution of BT-CF-Au₉/Pd₃.

Table 2

Content of Au and Pd at different points of a distinct NP in BT-CF-Au₉/Pd₁.

Location	Content of Au (%)	Content of Pd (%)
1	95.29	4.70
2	6.98	93.02
3	48.62	51.37

size of 10.63 ± 1.9 nm. EDS point analyses of a distinct NP in BT-CF-Au₉/Pd₁ is shown in Fig. 4. The contents of Au and Pd at each point are summarized in Table 2. Clearly, Au is rich in the interior of the particle, while Pd is mainly located at the edge of the particle. These results confirm a typical Au core/Pd shell structure of the NPs in the BT-CF-Au₉/Pd₁ catalyst. As proposed in Scheme 1c–e, when most of the phenolic hydroxyls of BT are consumed by the reductive adsorption of Au³⁺, the subsequently adsorbed Pd²⁺ will be mainly located on the negatively charged surface of Au NPs via electrostatic attraction, and then form Pd shell by the reduction of NaBH₄. Considering that the NPs in BT-CF-Au₉/Pd₁ have core–shell structure, the catalyst was denoted as BT-CF-Au₉@Pd₁ in the following text.

To further investigate the preparation mechanism of Au@Pd bimetallic catalyst, BT-CF-Au₉@Pd₃ was prepared according to the same procedures used for preparation of BT-CF-Au₉@Pd₁. The morphology and particle size distribution of Au₉@Pd₃ NPs are shown in Fig. 5. Roughly spherical NPs are still formed in BT-CF-Au₉@Pd₃, and the corresponding average particle size is 11.20 ± 2.7 nm, which is relatively larger than that of BT-CF-Au₉@Pd₁. This should be attributed to the formation of thicker Pd shell when a higher amount of Pd²⁺ is employed. To confirm this, high-resolution TEM (HRTEM) observation of BT-CF-Au₉@Pd₃ was carried out. As shown in Fig. 6, a distinct variation in contrast between the dark gold core and the lighter palladium shell was seen, while the lattice fringes of Pd cannot be observed, which suggests that the crystallinity of the Pd shell is quite low.

The XRD patterns of BT-CF-Pd, BT-CF-Au, BT-CF-Au₉@Pd₁ and BT-CF-Au₉@Pd₃ are shown in Fig. 7. As for BT-CF-Au, it exhibits an amorphous peak at 22° that belongs to the BT-CF supporting matrix. In addition, the characteristic peak of face centered cubic Au is clearly observed at 39.34°, which confirms the anchoring of highly crystallized Au NPs on the BT-CF. With regard to the bimetallic NPs with Au core/Pd shell structure (BT-CF-Au₉@Pd₁ and BT-CF-Au₉@Pd₃), the characteristic peaks of face centered cubic Au is still evident but its intensity is gradually decreased along with the increase of Pd content in the catalysts, which presents the core–shell nature of BT-CF-Au₉@Pd_x ($x = 1, 3$, respectively). In addition, the characteristic peak of Pd cannot be observed in the XRD patterns of all BT-CF-Au@Pd samples, which is possibly due to

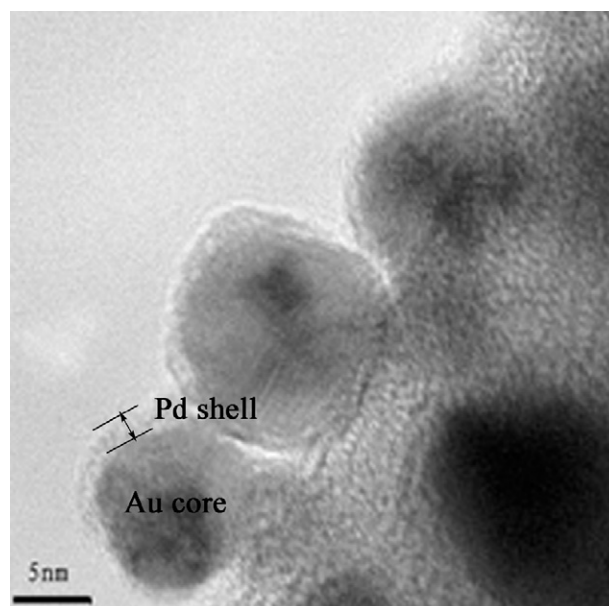


Fig. 6. Transmission electron micrographs of BT-CF-Au₉/Pd₃.

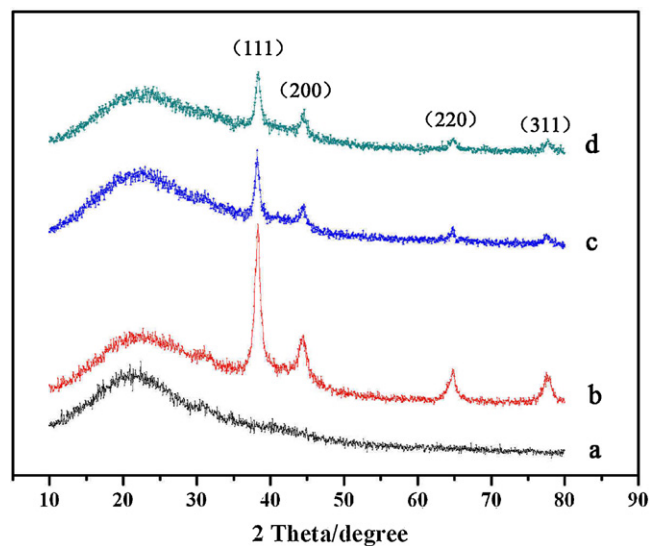


Fig. 7. XRD patterns of BT-CF-Pd (a), BT-CF-Au (b), BT-CF-Au₉@Pd₁ (c) and BT-CF-Au₉@Pd₃ (d).

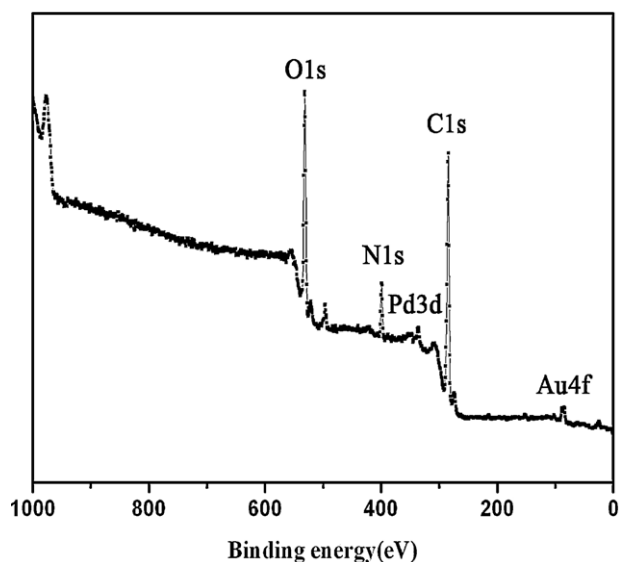


Fig. 8. Survey scan of BT-CF-Au₉@Pd₃ in the range of 0–1100 eV.

the fact that the crystallization of Pd shell is disturbed by the BT shell around the surface of the Au core.

The XPS survey scan spectrum of BT-CF-Au₉@Pd₃ is shown in Fig. 8. The main components of BT-CF-Au₉@Pd₃, such as O and C, exhibit strong absorption intensity, while Pd and Au show relatively weak absorption intensity because of their low content (0.43% and 0.59%, respectively). Subsequently, the XPS analyses of individual Au, Pd and O element in the BT-CF-Au₉@Pd₃ catalyst were carried out. As shown in Fig. 9a, the Au 4f XPS spectrum of BT-CF-Au₉@Pd₃ consists of two pairs of doublets from spin–orbital splitting of 4f_{7/2} and 4f_{5/2}. The spin–orbital splitting photoelectron was located at

binding energies of 84.2 and 87.8 eV, showing the presence of Au⁰ [14]. Another pair of doublets located at 85.0 and 89.0 eV should belong to Au oxides [15]. In Pd 3d XPS spectrum of BT-CF-Au₉@Pd₃ (Fig. 9b), two peaks located at 335.8 eV and 340.9 eV, which are attributed to elemental Pd. In Fig. 9d, the O 1s spectrum of BT-CF shows two peaks at 531.5 and 532.8 eV, which belong to the carbonyl oxygen (–C=O) and the phenolic hydroxyl oxygen (–C–OH), respectively. After anchoring Au/Pd NPs, a new peak appears at 533.6 eV, as shown in Fig. 9c, which confirms the electron donating/accepting interactions between BT and the NPs.

The surface morphology of the BT-CF-Au₉@Pd_x (x = 1, 3, respectively) catalyst is shown in supporting information 2. It can be observed that all the catalysts have well defined fibrous morphology, which suggests that the fibrous structure of the natural collagen fiber is well preserved in the BT-CF-Au₉@Pd_x catalysts. Compared with monolithic catalysts, fibrous catalysts have better geometric flexibility and lower mass transfer resistance [16,17], and thus often exhibit high catalytic activity. Actually, many efforts in recent years have been paid on the development of fibrous matrix supported catalysts because of the unique mass transfer property of this kind of catalysts [18–21]. From this view point, the high activity of the BT-CF-Au₉@Pd_x catalyst can be expected in the following catalytic experiments.

3.3. Activity evaluation of the BT-CF-Au/Pd catalyst

We chose cyclohexene as model molecule to investigate the catalytic activity of the BT-CF-Au/Pd catalysts. For comparison, the catalytic reaction was also carried out under the same conditions using BT-CF-Au and BT-CF-Pd as catalysts. The dependence of the conversion of cyclohexene on reaction time is shown in Fig. 10.

BT-CF-Au had no catalytic activity for the hydrogenation of cyclohexene under the experimental conditions. BT-CF-Pd was very active for the hydrogenation of cyclohexene, by which the substrate

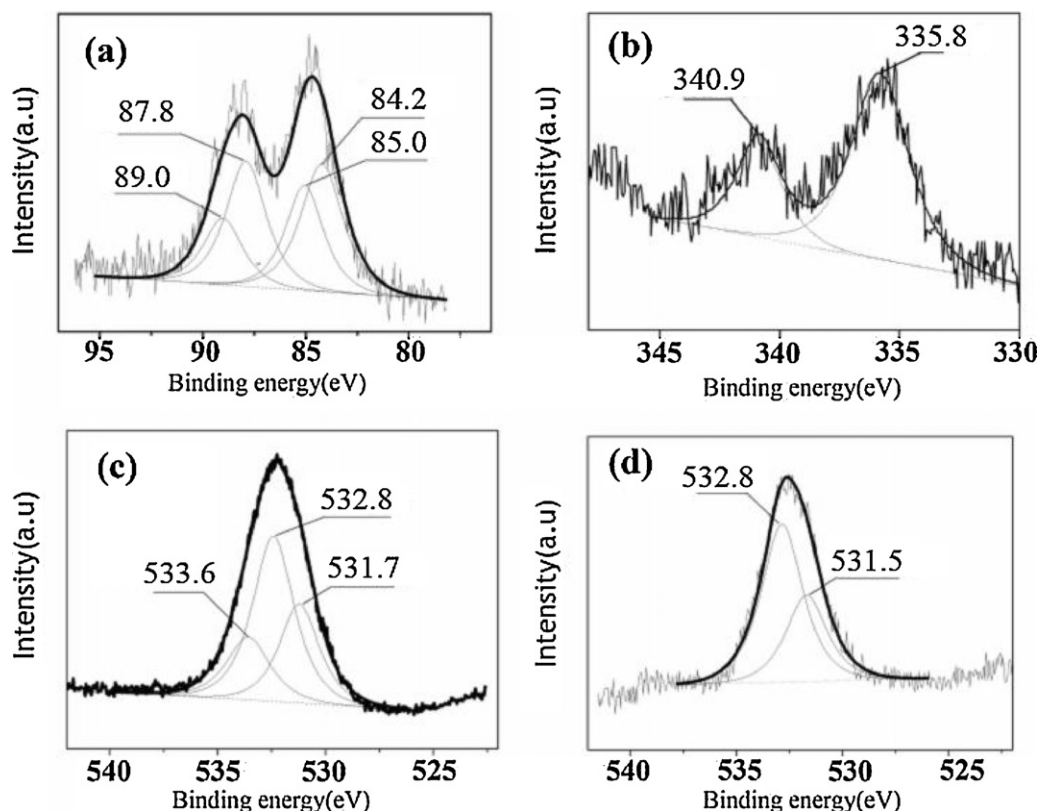
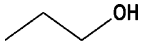
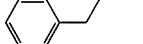
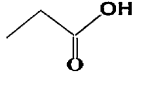
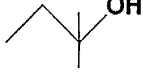
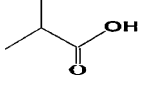
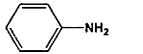
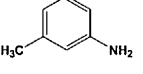
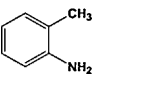


Fig. 9. Au 4f (a), Pd 3d (b) and O 1s XPS (c) spectra of BT-CF-Au₉@Pd₃, and O 1s XPS spectrum of BT-CF (d).

Table 3
Hydrogenation activity of BT-CF-Au₉@Pd₃ for other substrates.

Entry	Substrate	Product	Molar ratio (substrate/Pd)	TOF (mol mol ⁻¹ h ⁻¹)
1 ^a	Allyl alcohol		4000	10,980
2 ^a	styrene		4000	14,732
3 ^a	Acrylic acid		4000	10,262
4 ^a	2-Methyl-3-buten-2-ol		4000	6266
5 ^a	a-Methacrylic acid		2000	3624
6 ^b	Nitrobenzene		2000	1379
7 ^c	m-Nitrotoluene		2000	856
8 ^c	o-Nitrotoluene		2000	355

^a Solvent: methanol; pressure: 1 MPa H₂; temperature: 298 K.

^b Solvent: methanol; pressure: 1 MPa H₂; temperature: 313 K.

^c Solvent: methanol; pressure: 2 MPa H₂; temperature: 313 K.

conversion reached nearly 100% when the reaction was conducted for 92 min. As expected, BT-CF-Au₁/Pd₁ showed similar activity and the substrate was completely converted in 90 min. However, the catalytic activity of BT-CF-Au₉@Pd₁ and BT-CF-Au₉@Pd₃ were much higher than that of the BT-CF-Pd. When the BT-CF-Au₉@Pd₁ was used, the time needed for completing conversion of the substrate was reduced to 58 min, indicating an excellent synergy effect between Pd and Au for the reaction. Moreover, when BT-CF-Au₉@Pd₃ was employed as the catalyst, the time required for completing conversion of the substrate was further decreased to 40 min, which only counts for 1/3 of the reaction time required

by using the BT-CF-Pd catalyst. Compared with BT-CF-Au₉@Pd₁, the higher activity of BT-CF-Au₉@Pd₃ is due to the well structured core-shell of Au@Pd.

The operating stability of the as-prepared catalyst was further investigated, in comparison with that of commercial Pd/C catalyst. As showed in Fig. 11, the activity of the as-prepared BT-CF-Au₉@Pd₃ catalyst shows no significant loss of activity even re-used for 4 times in consideration of inevitable loss of catalyst during filtration, while the activity of commercial Pd/C catalyst was rapidly lost when re-used in the second time, which is probably due to the leaching of Pd species from the support. The satisfactory reusability

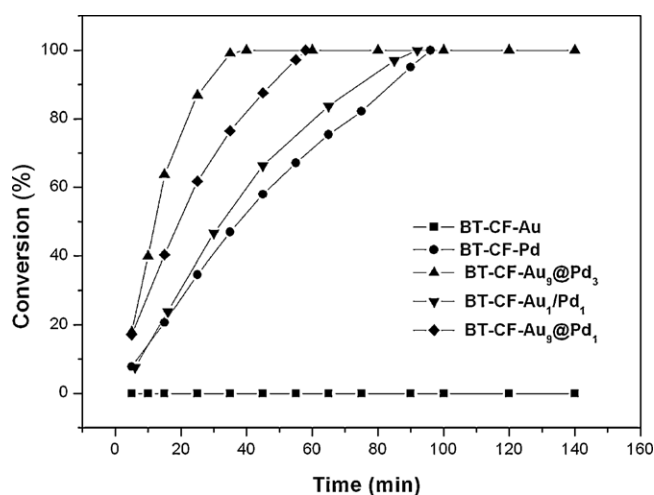


Fig. 10. Dependence of conversion of cyclohexene on reaction time over the BT-CF-Au/Pd catalysts. Reaction condition: metal Pd (2.5 μmol), cyclohexene (10 mmol), methanol (10 mL), temperature (298 ± 2 K) and pressure (1 MPa H₂).

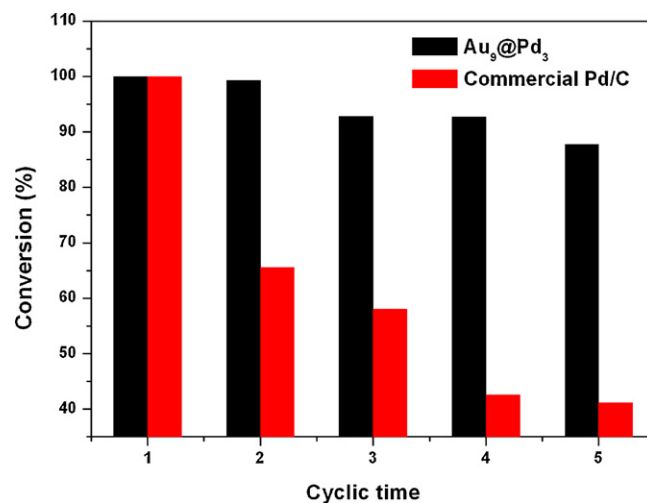


Fig. 11. Operating stability of BT-CF-Au₉@Pd₃ catalyst in catalytic hydrogenation of cyclohexene. Reaction condition: metal Pd (2.5 μmol), cyclohexene (10 mmol), methanol (10 mL), temperature (298 ± 2 K) and pressure (1 MPa H₂).

of the BT-CF-Au₉@Pd₃ catalyst should be attributed to the anchoring effect of phenolic hydroxyl of BT toward the metal NPs, which suppresses the agglomeration and leakage of NPs during catalytic reaction process.

To evaluate the universal application of BT-CF-Au₉@Pd₃ in liquid-phase hydrogenation, its catalytic activity for hydrogenation of some typical alkenes and nitro-compounds were tested. As shown in Table 3, BT-CF-Au₉@Pd₃ shows high catalytic hydrogenation activity for all the substrates containing C=C bond. The TOF of allyl alcohol, styrene and acrylic acid are 10,980, 14,732 and 10,262 mol mol⁻¹ h⁻¹, respectively (Entries 1–3). As expected, the presence of methyl-substitute causes a significant steric hindrance in the substrate, which leads to a decreased catalyst activity, as observed in hydrogenation of 2-methyl-3-buten-2ol and α -methacrylic acid (Entries 4 and 5). In addition, BT-CF-Au₉@Pd₃ is also effective for liquid-phase hydrogenation of nitro-compounds (Entries 6–8). For example, the TOF of nitrobenzene hydrogenation reaches 1379 mol mol⁻¹ h⁻¹ (Entry 6) when the reaction was conducted under 1 MPa H₂ at temperature 313 K with a substrate/Pd molar ratio of 2000.

4. Conclusion

Au/Pd bimetallic catalysts were successfully prepared by a seeding growth technique using tannin-grafted collagen fiber as supporting matrix. By proper controlling of molar ratio of Au/Pd, Au core/Pd shell NPs can be constructed exclusively on the fibrous collagen. Due to the synergy effect of Au and Pd, the as-prepared BT-CF-Au₉@Pd₃ catalyst exhibits much higher catalytic activity than the mono-metallic counterparts in liquid-phase hydrogenation of cyclohexene. The BT-CF-Au₉@Pd₃ catalyst can be re-used four times without significant loss of activity, exhibiting a better reusability than the commercial Pd/C catalyst. Moreover, the BT-CF-Au₉@Pd₃ catalyst also presents satisfactory catalytic activity to various alkenes and nitro-compounds.

Acknowledgments

We acknowledge the financial support provided by National High Technology Research and Development Program 863 of

China (2011AA08A108), Science and Technology Department of Sichuan Province, China (2010JY0056), and Education Department of Sichuan Province, China (09ZB065).

Appendix A. Supplementary data

Supplementary data associated with this article can be found, in the online version, at <http://dx.doi.org/10.1016/j.molcata.2012.07.028>.

References

- [1] A.U. Nilekar, S. Alayoglu, B. Eichhorn, M. Mavrikakis, *J. Am. Chem. Soc.* 132 (2010) 7418–7428.
- [2] X.H. Peng, Q.M. Pan, G.L. Rempel, *Chem. Soc. Rev.* 37 (2008) 1619–1628.
- [3] S. Alayoglu, P. Zavalij, B. Eichhorn, Q. Wang, A.I. Frenkel, P. Chupas, *ACS Nano* 3 (2009) 3127–3137.
- [4] S. Alayoglu, B. Eichhorn, *J. Am. Chem. Soc.* 130 (2008) 17479–17486.
- [5] T. Feng, E.G. Michael, Y.W. Zhang, R.R. James, Z. Liu, Y.C. Jen, S.M. Bongjin, S. Miquel, A.S. Gabor, *Science* 322 (2008) 932–934.
- [6] A.F. Lee, C.V. Ellis, K. Wilson, N.S. Hondow, *Catal. Today* 157 (2010) 243–249.
- [7] F.R. Fan, D.Y. Liu, Y.F. Wu, S. Duan, Z.X. Xie, Z.Y. Jiang, Z.Q. Tian, *J. Am. Chem. Soc.* 130 (2008) 6949–6951.
- [8] H. Mao, C. Chen, X.P. Liao, B. Shi, *J. Mol. Catal. A: Chem.* 341 (2011) 51–56.
- [9] D.H. Deng, R. Tang, X.P. Liao, B. Shi, *Langmuir* 24 (2008) 368–370.
- [10] H. Wu, R. Tang, Q. He, X.P. Liao, B. Shi, *J. Chem. Technol. Biotechnol.* 84 (2009) 1702–1711.
- [11] H.M. Chen, C.F. Hsin, R.S. Liu, J.F. Lee, L.Y. Jang, *J. Phys. Chem. C* 111 (2007) 5909–5914.
- [12] S. Iravani, *Green Chem.* 13 (2011) 2638–2650.
- [13] X. Huang, H. Wu, S.Z. Pu, W.H. Zhang, X.P. Liao, B. Shi, *Green Chem.* 13 (2011) 950–957.
- [14] J. Llorca, A. Casanovas, M. Domínguez, I. Casanova, I. Angurell, M. Seco, O. Rossell, *J. Nanopart. Res.* 10 (2008) 537–542.
- [15] E.D. Park, J.S. Lee, *J. Catal.* 186 (1999) 1–11.
- [16] E.V. Polienova, A.Y. Valdberg, *Chem. Petrol. Eng.* 46 (2010) 57–59.
- [17] X. An, J.L. Li, Y.Z. Zuo, Q. Zhang, D.Z. Wang, J.F. Wang, *Catal. Lett.* 118 (2007) 264–269.
- [18] J. Han, J. Dai, L.Y. Li, P. Fang, R. Guo, *Langmuir* 27 (2011) 2181–2187.
- [19] V. Polshettiwar, J.T. Cazat, M. Taoufik, F. Stoffelbach, S. Norsic, J.M. Basset, *Angew. Chem. Int. Ed.* 50 (2011) 2747–2751.
- [20] S. Takenaka, T. Iguchi, E. Tanabe, H. Matsune, M. Kishida, *Carbon* 47 (2009) 1251–1257.
- [21] A. Guha, T.A. Zawodzinski, D.A. Schiraldi, *J. Power Sources* 195 (2010) 5167–5175.